Oncogenic stress-induced Netrin reprograms systemic metabolism as a humoral inter-organ molecule in *Drosophila*

Morihiro Okada[*1,2], Tomomi Takano[1,2], Yuko Ikegawa[2,3], Hanna Ciesielski[1,4], Hiroshi Nishida[1,5], Sa Kan Yoo[*1,2,4]

[1]Physiological Genetics Laboratory, RIKEN CPR
[2]Laboratory for Homeodynamics, RIKEN BDR
[3]Graduate School of Biostudies, Kyoto University
[4]Division of Developmental Biology and Regenerative Medicine, Kobe University
[5]Division of Cell Physiology, Kobe University

*These authors equally contributed to this work.
Correspondence: morihiro.okada@riken.jp (M)), sakan.yoo@riken.jp (SKY),

Keywords
Netrin, oncogenic stress, inter-organ communication, *Drosophila*

Abstract

Cancer exerts pleiotropic, systemic effects on organisms (Bilder, Ong, Hsi, Adiga, & Kim, 2021; Hiam-Galvez, Allen, & Spitzer, 2021). Health of organisms with cancer deteriorates, eventually leading to organismal death. How cancer induces systemic effects on remote organs and the organism itself still remains elusive. Here we describe a role for NetrinB (NetB), a protein with a particularly well-characterized role as a tissue-level axon guidance cue (Bradford, Cole, & Cooper, 2009; Kennedy, 2000; Serafini et al., 1996), in mediating oncogenic stress-induced organismal, metabolic reprogramming as a systemic humoral factor. Ras-induced dysplasia upregulates and secretes NetB. Inhibition of either NetB from the transformed tissue or its receptor in the fat body suppresses oncogenic stress-induced organismal death. Mechanistically, NetB from the dysplastic tissue remotely suppresses carnitine biosynthesis, which is critical for acetyl-CoA generation and systemic metabolism, in the fat body. Supplementation of carnitine or acetyl-CoA inhibits oncogenic stress-induced organismal death. This is the first identification, to our knowledge, of a role for the Netrin molecule, which has been studied extensively for its role within tissues, in humorally mediating systemic effects of local oncogenic stress on remote organs and organismal metabolism.

Main

Why animals die from cancer is enigmatic. While cancer affects organs where it exists, cancer patients often exhibit systemic symptoms. For example, it has been long known that cancer patients tend to suffer from infection due to immunosuppression that often accompanies cancer (Bodey, 1986; Hanahan & Weinberg, 2011; Hiam-Galvez et al., 2021). Cancer also induces cachexia, which is defined by loss of muscles and fat tissues (Argiles, Busquets, Stemmler, & Lopez-Soriano, 2014). Metabolic dysfunction induced by tumor can be primary causes of cancer-related morbidity and mortality (Egeblad, Nakasone, & Werb, 2010).The cytokine storm has been postulated to mediate the cancer's systemic effects such as immunosuppression and cachexia (Argiles et al., 2014; Hiam-Galvez et al., 2021; Luft, 2007), but its exact mechanism remains elusive.

To understand how tumor affects organismal physiology and metabolism, we used *Drosophila* larvae, a genetically tractable system to study tumor biology (Bilder et al., 2021; Dar, Das, Shokat, & Cagan, 2012; Nishida et al., 2021; Santabarbara-Ruiz & Leopold, 2021; Villegas, 2019; Wu, Pastor-Pareja, & Xu, 2010). To prevent an occurrence of too strong a malignant situation such as metastasis or massive overproliferation, which has a tremendous local effect, arresting development and confounding interpretaion of the systemic effect, we decided to induce a relatively mild, pre-cancer situation, in the eye imaginal disc, which is a dispensable organ for organismal suvival. We expressed Ras^{V12}, which is the most common mutation and a prerequistie for many tumors (Hobbs, Der, & Rossman, 2016; Prior, Lewis, & Mattos, 2012), in the eye disc using the GMR enhancer elemtent (Freeman, 1996; Tang, Neufeld, Rubin, & Muller, 2001). Ras expression in the eye disc leads to dysplastic tissue, as previously demonstrated (Simon, Bowtell, Dodson, Laverty, & Rubin, 1991), which results in the "rough eye" in adults (Fig S1a-b). Although this dysplastic tissue does not metastasize or affect the brain tissue, it leads to high lethality: over 80% of the *GMR-*Ras^{V12} animals die (Fig 1a). Most of *GMR-*Ras^{V12} larvae pupariate without developmental delay compared to control flies in spite of oncogenic stress in the eye imaginal disc (Fig S1c). This is due to the late initiation of *GMR*-driven Ras expression behind the morphogenetic furrow (Freeman, 1996), past the timing when stresses can delay developmental timing (Halme, Cheng, & Hariharan, 2010). In spite of the high lethality, animals

carrying *Ras^{V12}* -transformed tissue do not display a cachexia symptom such as muscle or fat body degeneration, which is induced by more aggressive tumors (Ding et al., 2021; Figueroa-Clarevega & Bilder, 2015; Khezri et al., 2021; Kim et al., 2021; Kwon et al., 2015; Newton et al., 2020; Santabarbara-Ruiz & Leopold, 2021; Song et al., 2019).

Since the local event is relatively minor without metastasis or extensive overgrowth, we hypothesized that the dysplastic tissue that expresses Ras^{V12} may secrete humoral factors that could mediate systemic effects of the oncogenic stress, leading to organismal death. We performed RNA sequencing using the eye disc tissue from control and *GMR-Ras^{V12}* flies. Among the genes encoding secreted, we identified 20 secreted proteins that were highly upregulated in the eye disc from *GMR-Ras^{V12}* flies (Fig 1b). Among these, we found that inhibition of *NetrinB* (*NetB*) reverses the organismal lethality induced by Ras^{V12} (Fig 1c-d, Fig S1d-e). *NetB* inhibition did not reduce the eye size or the rough eye phenotype in *GMR-Ras^{V12}* flies (Fig S1f-h), suggesting that the local event is intact. Ectopic expression of *NetB* in the eye disc of normal animals induced lethality (Fig 1e). Consistent with the RNA-seq data, RT-qPCR confirmed that the eye disc of *GMR-Ras^{V12}* flies upregulates *NetB* mRNA (Fig 1f). The eye disc of *GMR-Ras^{V12}* flies also has higher levels of NetB protein (Fig 1g-i).

In mammals and flies, Netrin molecules play major roles in neuronal navigation during development of the nervous system (Bradford et al., 2009; Kennedy, 2000; Serafini et al., 1996). In addition, Netrin and its receptors have been implicated in tumorigenesis in some types of cancers (Arakawa, 2004; Hao et al., 2020; Kefeli et al., 2017). In general, Netrin molecules have been described to function within the tissue, and their humoral role has not been known. We speculated that, since NetB is secreted, it might work as a humoral factor. To test the hypothesis that NetB from the *GMR-Ras^{V12}* eye disc reaches remote organs, we examined non-tumor tissues. We found that NetB protein abundantly exists in the fat body of *GMR-Ras^{V12}* flies (Fig 2a-c). Importantly, endogenous expression of *NetB* mRNA in the fat body was unchanged in *GMR-Ras^{V12}* flies compared to control flies (Fig 2d), strongly suggesting that NetB protein observed in the fat body of *GMR-Ras^{V12}* flies is not due to its increased transcription. To completely exclude a possibility that NetB is generated in the

fat body, we made a transgenic line *UAS-NetB-GFP* to visualize the incorporation of NetB in the fat body. Ectopic expression of the GFP-tagged NetB, but not control GFP, in the eye disc led to existence of GFP signals in both the hemolymph and the fat body (Fig 2e-l, Fig S2a), providing further evidence that NetB secreted by the eye disc humorally relays the signal to the fat body. Furthermore, inhibition of a NetB receptor, Unc-5 in the fat body increased organismal survival over oncogenic stress (Fig 2m-n, Fig S2b-d), suggesting an involvement of NetB signaling in the fat body.

How does Netrin signaling regulate the fat body and organismal metabolism? To get a clue on Netrin-mediated signals, we performed RNAseq of the fat body with/without *GMR-Ras^{V12}* dysplasia. Importantly, because in a different line of research, we had already obtained data that insulin signaling inhibition in the fat body enhances organismal survival of *GMR-Ras^{V12}* flies, phenocopying the Netrin inhibition, potentially through downregulation of the NetB receptor *unc-5* (Fig 3a, Fig S3a-j), we focused on genes that are regulated by Ras and reversed by insulin inhibition. Among such genes is trimethyllysine hydroxylase, epsilon (TMLHE), which regulates the carnitine biosynthesis pathway (Maas, Hintzen, Porzberg, & Mecinovic, 2020). Both RNAseq and RT-qPCR demonstrated that *TMLHE* mRNA is decreased in the fat body of *GMR-Ras^{V12}* flies and increased by InR knockdown in the fat body (Fig 3b-c). Importantly, *NetB* inhibition in the Ras-transformed eye disc reversed the Ras-dependent *TMLHE* downregulation in the fat body (Fig 3d). Further, only *unc-5* but not other Netrin receptor knockdown affected *TMLHE* expression (Fig 3e, Fig S3k-l), suggesting that Unc-5 mainly mediates the NetB signal in the fat body.

TMLHE plays an important role in carnitine biosynthesis and hence acetyl-CoA production from fatty acids (Fig 4a). Consistently, the amount of carnitine is decreased in the fat body of *GMR-Ras^{V12}* flies compared to control (Fig. 4b). we tested whether manipulation of TMLHE in the fat body could affect organismal death. Knockdown of *TMLHE* in the fat body of *GMR-Ras^{V12}* flies significantly decreased their survival (Fig 4c, Fig S4a-d), suggesting that inhibition of *TMLHE* in the fat body makes animals more sensitive to Ras-transformation. In the absence of *GMR-Ras^{V12}*, inhibition of *TMLHE* in the fat body is not sufficient to induce organismal death (Fig S4e-g), suggesting an oncogenic stress-specific role for TMLHE.

To further investigate the involvement of carnitine and acetyl-CoA, a critical metabolite for energy production, in survival of *GMR-Ras^{V12}* flies, we orally supplemented carnitine or acetyl-CoA. Since highly charged acetyl-CoA is a membrane-impermeant molecule in general, we fed acetate as an acetyl-CoA precursor (Comerford et al., 2014; Pietrocola, Galluzzi, Bravo-San Pedro, Madeo, & Kroemer, 2015). Carnitine or the acetyl-CoA precursor administration enhanced survival of *GMR-Ras^{V12}* flies (Fig 4d-e) and reversed the effect of *TMLHE* knockdown (Fig 4f). Taken together, the Ras-transformed tissue remotely inhibits carnitine biosynthesis in the fat body, which reduces acetyl-CoA production, inducing organismal lethality.

We finally tested a generality of our findings in a different oncogenic system. We focused on a tumor model in the adult gut (Apidianakis, Pitsouli, Perrimon, & Rahme, 2009; Markstein et al., 2014; Tsuda-Sakurai, Kimura, & Miura, 2020). We generated a dual genetic system that enabled *Ras^{V12}* expression in adult intestinal stem cells by the *esg-LexA*::*HG* driver and gene manipulation in the fat body by the *Cg-Gal4* driver (Fig S5a). As previously shown (Apidianakis et al., 2009; Markstein et al., 2014; Tsuda-Sakurai et al., 2020), *Ras^{V12}* expression induces hyperplasia of the gut epithelia, which is detected by the enhanced phospho-Histone3 (pH3)-positive cell number (Fig S5b-e). Flies with the intestinal Ras tumor die much earlier than control (Fig S5f). Knockdown of *TMLHE* in the adult fat body aggravated survival of *esg^{ts}>Ras^{V12}* flies without perturbing tumor proliferation (Fig 4g, Fig S5b-e), suggesting that carnitine generation in the fat body is also important for survival in the adult tumor situation.

Here we reveal a mechanism by which local oncogenic stress affects organismal death: Ras-induced dysplastic tissues secrete NetB, which humorally inhibits *TMLHE* expression in the fat body, leading to reduction of carnitine biosynthesis (Fig 4h). Since Netrin molecules could play local roles in tumorigenesis, they are potential therapeutic targets for cancer treatment (Arakawa, 2004; Hao et al., 2020; Kefeli et al., 2017). Nentrin-1 protein levels in the plasma are increased in various cancer patients, which has been noted as a cancer marker without functional implications in its systemic role (Ko, Blatch, & Dass, 2014). On the other hand, serum carnitine levels become low in human

cancer patients (Silverio, Laviano, Rossi Fanelli, & Seelaender, 2011). Our findings in *Drosophila* imply a possibility that these two, at a glance unrelated symptoms could be mechanistically linked. If our findings are applicable to humans, inhibition of Netrin signaling in cancer patients may kill two birds with one stone, by improving the systemic symptom as well as by suppressing local tumorigenesis.

One question is why Ras-transformed tissues actively secrete NetB to suppress carnitine production in the fat body. Considering that the organismal response to oncogenic stress, especially such a mechanism that induces organismal lethality, likely has not been evolutionarily selected, we speculate that humorally mediated NetB signaling in the fat body may play an alternative, more adaptive role in a more physiological context, which Ras-transformed tissues hijack accidently. We hypothesize that NetB signaling evolved to couple and coordinate two events simultaneously: local neurogenesis and systemic metabolism, both of which oncogenic tissues could take advantage of.

Figure Legend

Fig. 1 NetrinB in Ras^{V12} transformed tissues affects organismal lethality

a, Expression of oncogenic *Ras^{V12}* under the control of *GMR* enhancer element (*GMR-Ras^{V12}*) leads to organismal lethality. The survival rate is calculated by counting the number of adult flies.

b, Expression of selected genes that were upregulated in the eye disc of *GMR-Ras^{V12}* flies.

c, Knockdown of *NetB* in the eye disc of *GMR-Ras^{V12}* flies enhances survival.

d, *NetB* heterozygous mutant flies survive better over Ras^{v12}-induced oncogenic stress.

e, Ectopic expression of *NetB* in the eye disc kills animals even without tumor formation in the eye.

f, qRT-PCR with mRNA from the eye disc confirms higher expression of *NetB* in *GMR-Ras^{V12}* flies

g-h, Oncogenic *Ras* expression in the eye disc induces NetB protein, which was detected by GFP signal using CPTI-000748, a protein trap of NetB.

i, Quantification of GFP signals in **g** and **h**.

Data are mean ± s.e.m. and the statistical significance was determined by one-way ANOVA followed by Tukey's multiple comparison test (**c**) and two-tailed unpaired *t*-test (**a, d, e, f, and i**). Scale bar, 50 μm.

Fig. 2 NetB secreted from the eye dysplasia functions in the fat body.
a-b, The amount of NetB protein increases in the fat body *GMR-Ras^{V12}* (**a**) compared to control flies (**b**). CPTI-000748, a protein trap of NetB, labels endogenous NetB.
c, Quantification of mean intensity of GFP signals in **a** and **b**.
d, There is no difference of *NetB* mRNA expression in the fat body of *GMR-Ras^{V12}* and control flies.
e-h, Ectopic expression of GFP-tagged NetB in the eye disc induces high levels GFP-NetB protein in the fat body.
i, Quantification of mean intensity of GFP signal in the fat body of **f** and **h**.
j-k, Ectopic expression of GFP-tagged NetB in the eye disc leads to detection of GFP signals in the hemolymph.
l, Quantification of median intensity of GFP signals in **j** and **k**.
n, Knockdown of *unc-5*, NetB receptor, in the fat body increases organismal survival over the oncogenic stress.
o, *unc-5* heterozygous mutants flies survive better over Ras^{v12}-induced oncogenic stress.
Data are mean ± s.e.m. and the statistical significance was determined using a two-tailed unpaired *t*-test (**c**, **d**, **i**, and **l-o**).

Fig. 3. **NetB regulates *TMLHE* expression through Unc-5 in the fat body of *GMR-Ras^{V12}* flies**
a, Knockdown of InR (InR) or expressing a dominant-negative form of InR (InR-DN) in the fat body using *CG-Gal4* increases survival over oncogenic *Ras* expression in the imaginal disc.
b, Expression of selected gene that were down-regulated in the fat body of *GMR-Ras^{V12}* flies and up-regulated by inhibition of insulin signals (*GMR-Ras^{V12}, CG-Gal4>InR-DN*).
c, qRT-PCR demonstrates that *TMLHE* expression in the fat body is reduced by *Ras* expression in the eye disc and reversed by insulin inhibition in the fat body.
d, qRT-PCR demonstrates that *NetB* knockdown in the eye disc increases *TMLHE* expression in the fat body.

e, Knockdown of *unc-5*, but not other NetB receptors (*Fra* or *Dscam1*), in the fat body increases *TMLHE* expression.
Data are mean ± s.e.m. and n represents the number of flies that were analyzed. The statistical significance was determined by one-way ANOVA followed by Tukey's multiple comparison test (**a**, **c**, and **e**), two-tailed unpaired *t*-test (**d**).

Fig. 4. **Carnitine biosynthesis is reduced in the fat body of *GMR-Ras^{V12}* flies**
a, A schematic of carnitine biosynthesis and its role to transport acyl-CoA to mitochondria.
b, Local expression of oncogenic *Ras* in the eye disc decreases the amount of carnitine in the fat body.
c, *TMLHE* knockdown in the fat body aggravates organismal survival over the oncogenic stress.
d. Carnitine feeding increases the survival rate over the oncogenic stress.
e, Acetyl-CoA precursor (acetate) administration makes *GMR-Ras^{V12}* flies survive.
f, Feeding of acetyl-CoA precursor (acetate) makes *GMR-Ras^{V12}* flies survive even with *TMLHE* knockdown in the fat body.
g, Knockdown of *TMLHE* in the fat body in adult flies shortened lifespan of *esg^{ts}>Ras^{V12}* flies.
h, A schematic of the proposed model. Ras^{V12} transformed tissue-derived NetB reprograms organismal metabolism through downregulation of carnitine biosynthesis in the fat body.
Data are mean ± s.e.m. and n represents the number of flies that were analyzed. The statistical significance was determined by two-tailed unpaired *t*-test (**b**-**f**), log-rank (Mantel-Cox) test (**g**).

Fig S1 *GMR-Ras^{V12}* model and *NetB* expression
a-b, Representative images of adult eyes from OregonR (**a**) and *GMR-Ras^{V12}* flies (**b**).
c, No developmental retardation for the timing of pupariation was observed in *GMR-Ras^{V12}* flies. The time for each larva to reach a pupal stage was determined and plotted. AED, hours after egg deposition.

d-e, qRT-PCR analysis of *NetB* RNAi efficiency. NetB RNAis lowered expression of *NetB* mRNA.
f-g, Representative images of adult eyes from *GMR-Ras^{V12}* flies with (**g**) or without knockdown (**f**) of *NetB* in the eye disc using *GMR-Gal4*.
h, Quantification of the eye area in **f** and **g**.
Data are mean ± s.e.m. and n represents the number of larvae that were analyzed. The statistical significance was determined using a two-tailed unpaired *t*-test (**d**, **e**, and **h**). Scale bar, 100 μm.

Fig S2 NetB in the hemolymph and knockdown of *unc-5*
a, Ectopic expression of GFP-tagged NetB in the eye disc leads to GFP signals, which were detected by a spectrophotometer, in the hemolymph.
b, Knockdown of *unc-5* in the fat body increases survival of *GMR-Ras^{V12}* flies.
c-d, qRT-PCR analysis of *unc-5* RNAi efficiency. *unc-5* RNAis lowered the expression of *unc-5* mRNA.
Data are mean ± s.e.m. and the statistical significance was determined using a two-tailed unpaired *t*-test (**a**-**d**).

Fig S3 Insulin inhibition increases survival of *GMR-Ras^{V12}* flies.
a, *Dilp* heterozygous mutants survive better over oncogenic *Ras* expression in the imaginal disc.
b, Expression of a dominant-negative form of insulin receptor (InR-DN) in the fat body (*CG-Gal4*, *FB-Gal4*) but not in other tissues increases survival over oncogenic *Ras* expression in the imaginal disc. We used the following *Gal4* lines: *GMR-Gal4* (eye disc), *nub-Gal4* (wing disc), *esg*-Gal4 (gut; intestinal stem cells), *Mef2-Gal4* (somatic muscle), *promE-Gal4* (oenocyte), *CG-Gal4* (fat body), and *FB-Gal4* (fat body).
c, Knockdown of InR (InR) or expressing a dominant-negative form of InR (InR-DN) in the fat body using *FB-Gal4* driver increases survival over oncogenic *Ras* expression in the imaginal disc.
d-f, InR manipulation in the fat body does not affect the eye disc.
Representative images of adult eyes and wings from *GMRRas^{V12}*, *CG-Gal4>+* (**d**), *GMR-Ras^{V12}*, *CG-Gal4>InR-RNAi* (**e**), and *GMR-Ras^{V12}*, *CG-Gal4>InR-DN* (**f**).
g, Quantification of the eye area in **d-f**. The adult eye area was measured and normalized against the adult wing area.

h-i, InR knockdown in the fat body does not induce developmental delay. The time for each larva to reach the pupal stage (**h**) and the duration of pupal-adult development for each pupa (**i**) was determined and plotted. AED, hours after egg deposition.
j, qRT-PCR analysis of *unc-5* expression in the fat body. *unc-5* mRNA was significantly increased in the fat body of *GMR-Ras^{V12}* flies and this was reversed by fat body-specific expression of InR-DN.
k-l, qRT-PCR analysis of RNAi efficiency of *fra* (**k**) and *Dscam1* (**l**).
Data are mean ± s.e.m. and the statistical significance was determined by one-way ANOVA followed by Tukey's multiple comparison test (**a**-**c**, **g**, **i**, and **j**) and two-tailed unpaired *t*-test (**k**, **l**). Scale bar, 100 μm.

Fig S4 *TMLHE* knockdown in the fat body
a-b, Knockdown of *TMLHE* in the fat body of *GMR-Ras^{V12}* flies aggravates organismal survival, demonstrated by using a different RNAi line (**a**) or another fat body-specific *FB-Gal4* driver (**b**).
c-d, qRT-PCR analysis of *TMLHE* RNAi efficiency. *TMLHE* RNAis lowered expression of *TMLHE* mRNA.
e-g, In the absence of tumor burden, inhibition of *TMLHE* in the fat body does not affect organismal death. *TMLHE* was inhibited by *TMLHE* RNAis using *CG-Gla4* (**e**, **f**) and *FB-Gla4* driver (**g**).
Data are mean ± s.e.m. and the statistical significance was determined using a two-tailed unpaired *t*-test (**a**-**g**).

Fig S5 Gut tumor model in adult flies
a, Illustration of the gut tumor model in adult fles. *esg*-LexA::HG drives Ras^{V12} in intestinal stem cells and *CG-Gal4* drives genes of interest in the fat body. Both *LexA*- and *Gal4*-induced expression is regulated by a temperature through *Gal80^{ts}*.
b-d, Representative images of *Drosophila* adult stained for DAPI (Nuclei)(**b**-**d**) and pH3 (cell proliferation) (**b'**-**d'**). Transgenes were induced with *esg^{ts}* by incubating flies at 30 °C for 1day.
e, Quantification of the number of pH3-positive cells per gut in **b**-**d.**
f, Expression of oncogenic *Ras* in the adult gut using the *esg-LexA* driver shortens lifespan compared to control flies.

Data are mean ± s.e.m. and n represents the number of flies that were analyzed. The statistical significance was determined by one-way ANOVA followed by Tukey's multiple comparison test (**e**) and log-rank (Mantel-Cox) test (**f**). Scale bar, 20μm.

Table 1 Fly stock information
Table 2 Primer information

Methods

Fly stocks

Fly stocks used in this study are shown in Table1.

Drosophila husbandry and feeding assay

Flies were maintained as previously described (Yoo et al., 2016). The fly food is composed of the following ingredients: 0.8% agar, 10% glucose, 4.5% corn flour, 3.72% dry yeast, 0.4% propionic acid, 0.3% butyl p-hydroxybenzoate. For acetate supplementation experiments, acetate (FUJIFILM Wako) was added to the fly food to a final concentration of 333 or 500 mM. Carnitine (Tokyo Chemical Industry) was also added to the fly food to a final concentration of 100 mM.

Plasmid construction and transgenesis

The cDNA encoding NetB was amplified with Phusion High-Fidelity DNA polymerase (Thermo Fisher Scientific) and subcloned into the pEGFP-N1vector (Addgene) by KpnI/EcoRI. Then, NetB-EGFP fragment was subcloned into the pJFRC7-20XUAS-IVS-mCD8-GFP vector (Addgene) by XhoI/Xba. The plasmid inserted into the attP2 site using phiC31-mediated transgenesis (Best Gene).

Measurement of the survival rate and developmental timing

Measurement of the survival rate was performed as previously (Nishida et al., 2021). After mated females were allowed to lay eggs on grape agar plates for 24 hours at 25°C, L1 stage larvae were collected from grape agar plates and placed into treatment vials with different food conditions (50 larvae/vial). The number of adult flies of each genotype that could eclose was recorded. Survival rates were calculated as the number of adult flies that eclosed divided by the expected number of larvae of each genotype placed in each vial. For developmental timing assay, the number of larvae that had pupariated was recorded at the indicated time points after egg deposition (AED). Most experiments were performed at 25°C, except the ones performed to increase the sensitivity of the assays at 23°C in Figs.1c, 3c and 3f or 30°C in Figs.1e, S1d-e, S2c-d, 3k, S3l-m, S4c-d, and S5b-f.

Quantification of the eye and wing size

Left/right eyes and wings were dissected from adult flies. Bright view photographs were taken by using a digital CCD color camera (Nikon Digital Sight DS-Fi2) attached to a Nikon SMZ18 stereomicroscope (Nikon Instruments Inc.). The eye and wing areas were manually traced and measured using ImageJ software (National Institutes of Health).

RNA-sequencing

Total RNA was isolated from the fat body and the eye disc from L3 stage larvae with indicated genotypes using the RNeasy Mini Kit (Qiagen). Library construction and sequencing for the eye disc were carried out by Macrogen Japan Corp. RNA-seq libraries for the fat bodies were prepared using the TruSeq Stranded mRNA Sample Prep Kit (Illumina). The prepared libraries were sequenced by the HiSeq 1500. The obtained reads were mapped and analyzed by CLC Genomics Workbench version 20.0.4 software (Filgen). The expression heat maps were drawn using the online program Heatmapper (Babicki et al., 2016).

Quantitative RT-PCR (qRT-PCR)

Quantitative RT-PCRs were performed as described (Okada & Shi, 2018). Briefly, Total RNA was isolated from the fat body, eye disc, and whole body from L3 stage larvae using the Maxwell RSC simplyRNA Tissue Kit (Promega). The reverse transcription (RT) reaction was carried out using the ReverTra Ace qPCR RT Kit (Toyobo). The resulting cDNA was diluted 1:5, and the diluted products (2 µl) were subjected to PCR by using a FastStart Essential DNA Green Master Mix (Roche) in a 10 µl of reaction solution and the LightCycler 96 (Roche) according to the manufacturer's protocol. The level of mRNAs was normalized against the level of RpL32 mRNA for each sample. Primers used for qRT-PCRs are shown in Table2.

Immunofluorescence and imaging

For immunostaining, the eye imaginal disc, the fat body, and adult midguts were dissected in PBS, fixed with paraformaldehyde in PBS, and washed in PBS with 0.1% Triton X-100, according to the method described previously (Sasaki, Nishimura, Takano, Naito, & Yoo, 2021). The following reagents were used at indicated dilution: DAPI (1:500; D9542, Sigma), rabbit-anti-phospho-H3 (1:200; 06–570, Merck), Alexa rabbit Fluor 568 secondary antibody (1:500; A-11036, Thermo Fisher), and GFP-Booster Alexa Fluor® 488 (1:200; gb2AF488-50, Chromotek). For lipid droplet staining, fat bodies were stained with Lipi-Red (1:1000; LD03, Dojindo Molecular Technologies). Fluorescence images were acquired with a confocal microscope (Zeiss LSM 880, 900) as previously described (Ciesielski et al., 2022). Quantification of the intensity measurement of fluorescent signals was performed by ImageJ software (National Institutes of Health) or IMARIS 9.5.1 (Bitplane).

Measurement of carnitine in the fat body

Measurement of carnitine in the fat body were performed by using ultra-high-performance liquid chromatography with tandem mass spectrometry (UPLC-MS/MS). The fat bodies from two larvae at the L3 stage were used per sample and samples were processed according to previous description (Nishida et al., 2021). The detection was carried out on a XEVO TQ-S triple quadrupole tandem mass spectrometer coupled with electrospray ionization source (Waters). Precursor ion was scanned at m/z (MH+: 162.073 > 102.825 for Carnitine) by multiple reaction monitoring and established methods using individual authentic compounds and biological samples. The peak area of a target metabolite was analyzed using MassLynx 4.1 software (Waters). The insoluble pellets were heat-denatured with 0.2 N NaOH and used to quantify total protein using a BCA protein assay kit (Thermo).

Measurement of GFP signals in the hemolymph

GFP signals in the hemolymph were measured by either microscopy or spectrophotometry. For GFP signal measurement using a microscope, the hemolymph from ten larvae at the L3 stage was collected and spread onto a glass slide. Then, fluorescent images of the hemolymph were acquired using Zeiss LSM 900 confocal microscope. For GFP signal measurement using a Nanodrop spectrophotometer (Thermo Scientific), the hemolymph from three larvae at the L3 stage was collected and then measured for the absorbance at 509 nm. The standard curve was generated for each trial.

Statistical analysis.

All the statistical analyses were performed using Graphpad Prism 8. Data are presented as mean ± S.E. M. A two-tailed unpaired *t*-test was used to test between two samples. One-way ANOVA with multiple comparison tests was used to compare among group. Log rank (Mantel-Cox) test was used for comparison of survival distributions. Statistical significance is shown by asterisk; *P<0.05, ** P <0.01, *** P <0.001, **** P <0.0001.

Author contributions

Conceptualization: Sa Kan Yoo, Morihiro Okada
Formal analysis: Morihiro Okada, Tomomi Takano, Yuko Ikegawa, Hanna Ciesielski, Hiroshi Nishida, Sa Kan Yoo
Investigation: Morihiro Okada, Tomomi Takano, Yuko Ikegawa, Hanna Ciesielski, Hiroshi Nishida, Sa Kan Yoo
Methodology: Morihiro Okada, Tomomi Takano, Yuko Ikegawa, Hanna Ciesielski, Hiroshi Nishida, Sa Kan Yoo
Writing: Sa Kan Yoo, Morihiro Okada
Funding acquisition: Sa Kan Yoo, Morihiro Okada

Acknowledgement
We thank Iswar Hariharan, Takashi Nishimura, Masayuki Miura, Joel Levine and Shigeo Hayashi, and TRiP at Harvard Medical School, the Bloomington Stock Center and the VDRC stock center for fly stocks. We thank the Yoo lab members, Takashi Nishimura and Iswar Hariharan for their helpful comments on the manuscript. This work was supported by AMED-PRIME (17939907), the JSPS KAKENHI (JP16H06220, JP22H02807) and JST FOREST (JPMJFR216F) to S.K.Y.; KAKENHI (JP18K15021, 21K07138) and Sasagawa Scientific Research Grant from The Japan Science Society to M.O.

Competing interests
The authors declare no competing financial interests.

Corresponding authors
Morihiro Okada (morihiro.okada@riken.jp)
Sa Kan Yoo (sakan.yoo@riken.jp)

Apidianakis, Y., Pitsouli, C., Perrimon, N., & Rahme, L. (2009). Synergy between bacterial infection and genetic predisposition in intestinal dysplasia. *Proc Natl Acad Sci U S A, 106*(49), 20883–20888. doi:10.1073/pnas.0911797106

Arakawa, H. (2004). Netrin-1 and its receptors in tumorigenesis. *Nat Rev Cancer, 4*(12), 978–987. doi:10.1038/nrc1504

Argiles, J. M., Busquets, S., Stemmler, B., & Lopez-Soriano, F. J. (2014). Cancer cachexia: understanding the molecular basis. *Nat Rev Cancer, 14*(11), 754–762. doi:10.1038/nrc3829

Babicki, S., Arndt, D., Marcu, A., Liang, Y., Grant, J. R., Maciejewski, A., & Wishart, D. S. (2016). Heatmapper: web-enabled heat mapping for all. *Nucleic Acids Res, 44*(W1), W147–153. doi:10.1093/nar/gkw419

Bilder, D., Ong, K., Hsi, T. C., Adiga, K., & Kim, J. (2021). Tumour-host interactions through the lens of Drosophila. *Nat Rev Cancer, 21*(11), 687–700. doi:10.1038/s41568-021-00387-5

Bodey, G. P. (1986). Infection in cancer patients. A continuing association. *Am J Med, 81*(1A), 11–26. doi:10.1016/0002-9343(86)90510-3

Bradford, D., Cole, S. J., & Cooper, H. M. (2009). Netrin-1: diversity in development. *Int J Biochem Cell Biol, 41*(3), 487–493. doi:10.1016/j.biocel.2008.03.014

Ciesielski, H. M., Nishida, H., Takano, T., Fukuhara, A., Otani, T., Ikegawa, Y., . . . Yoo, S. K. (2022). Erebosis, a new cell death mechanism during homeostatic turnover of gut enterocytes. *PLoS Biol, 20*(4), e3001586. doi:10.1371/journal.pbio.3001586

Comerford, S. A., Huang, Z., Du, X., Wang, Y., Cai, L., Witkiewicz, A. K., . . . Tu, B. P. (2014). Acetate dependence of tumors. *Cell, 159*(7), 1591-1602. doi:10.1016/j.cell.2014.11.020

Dar, A. C., Das, T. K., Shokat, K. M., & Cagan, R. L. (2012). Chemical genetic discovery of targets and anti-targets for cancer polypharmacology. *Nature, 486*(7401), 80-84. doi:10.1038/nature11127

Ding, G., Xiang, X., Hu, Y., Xiao, G., Chen, Y., Binari, R., . . . Song, W. (2021). Coordination of tumor growth and host wasting by tumor-derived Upd3. *Cell Rep, 36*(7), 109553. doi:10.1016/j.celrep.2021.109553

Egeblad, M., Nakasone, E. S., & Werb, Z. (2010). Tumors as organs: complex tissues that interface with the entire organism. *Dev Cell, 18*(6), 884-901. doi:10.1016/j.devcel.2010.05.012

Figueroa-Clarevega, A., & Bilder, D. (2015). Malignant Drosophila tumors interrupt insulin signaling to induce cachexia-like wasting. *Dev Cell, 33*(1), 47-55. doi:10.1016/j.devcel.2015.03.001

Freeman, M. (1996). Reiterative use of the EGF receptor triggers differentiation of all cell types in the Drosophila eye. *Cell, 87*(4), 651-660. doi:10.1016/s0092-8674(00)81385-9

Halme, A., Cheng, M., & Hariharan, I. K. (2010). Retinoids regulate a developmental checkpoint for tissue regeneration in Drosophila. *Curr Biol, 20*(5), 458-463. doi:10.1016/j.cub.2010.01.038

Hanahan, D., & Weinberg, R. A. (2011). Hallmarks of cancer: the next generation. *Cell, 144*(5), 646-674. doi:10.1016/j.cell.2011.02.013

Hao, W., Yu, M., Lin, J., Liu, B., Xing, H., Yang, J., . . . Zhu, Y. (2020). The pan-cancer landscape of netrin family reveals potential oncogenic biomarkers. *Sci Rep, 10*(1), 5224. doi:10.1038/s41598-020-62117-5

Hiam-Galvez, K. J., Allen, B. M., & Spitzer, M. H. (2021). Systemic immunity in cancer. *Nat Rev Cancer, 21*(6), 345-359. doi:10.1038/s41568-021-00347-z

Hobbs, G. A., Der, C. J., & Rossman, K. L. (2016). RAS isoforms and mutations in cancer at a glance. *J Cell Sci, 129*(7), 1287-1292. doi:10.1242/jcs.182873

Kefeli, U., Ucuncu Kefeli, A., Cabuk, D., Isik, U., Sonkaya, A., Acikgoz, O., . . . Uygun, K. (2017). Netrin-1 in cancer: Potential biomarker and therapeutic target? *Tumour Biol, 39*(4), 1010428317698388. doi:10.1177/1010428317698388

Kennedy, T. E. (2000). Cellular mechanisms of netrin function: long-range and short-range actions. *Biochem Cell Biol, 78*(5), 569-575. Retrieved from https://www.ncbi.nlm.nih.gov/pubmed/11103947

Khezri, R., Holland, P., Schoborg, T. A., Abramovich, I., Takats, S., Dillard, C., . . . Rusten, T. E. (2021). Host autophagy mediates organ wasting and nutrient mobilization for tumor growth. *EMBO J, 40*(18), e107336. doi:10.15252/embj.2020107336

Kim, J., Chuang, H. C., Wolf, N. K., Nicolai, C. J., Raulet, D. H., Saijo, K., & Bilder, D. (2021). Tumor-induced disruption of the blood-brain barrier promotes host death. *Dev Cell, 56*(19), 2712-2721 e2714. doi:10.1016/j.devcel.2021.08.010

Ko, S. Y., Blatch, G. L., & Dass, C. R. (2014). Netrin-1 as a potential target for metastatic cancer: focus on colorectal cancer. *Cancer Metastasis Rev, 33*(1), 101-113. doi:10.1007/s10555-013-9459-z

Kwon, Y., Song, W., Droujinine, I. A., Hu, Y., Asara, J. M., & Perrimon, N. (2015). Systemic organ wasting induced by localized expression of the secreted insulin/IGF antagonist ImpL2. *Dev Cell, 33*(1), 36-46. doi:10.1016/j.devcel.2015.02.012

Luft, F. C. (2007). Cachexia has only one meaning. *J Mol Med (Berl), 85*(8), 783-785. doi:10.1007/s00109-007-0231-0

Maas, M. N., Hintzen, J. C. J., Porzberg, M. R. B., & Mecinovic, J. (2020). Trimethyllysine: From Carnitine Biosynthesis to Epigenetics. *Int J Mol Sci, 21*(24). doi:10.3390/ijms21249451

Markstein, M., Dettorre, S., Cho, J., Neumuller, R. A., Craig-Muller, S., & Perrimon, N. (2014). Systematic screen of chemotherapeutics in Drosophila stem cell tumors. *Proc Natl Acad Sci U S A, 111*(12), 4530-4535. doi:10.1073/pnas.1401160111

Newton, H., Wang, Y. F., Camplese, L., Mokochinski, J. B., Kramer, H. B., Brown, A. E. X., . . . Hirabayashi, S. (2020). Systemic muscle wasting and coordinated tumour response drive tumourigenesis. *Nat Commun, 11*(1), 4653. doi:10.1038/s41467-020-18502-9

Nishida, H., Okada, M., Yang, L., Takano, T., Tabata, S., Soga, T., . . . Yoo, S. K. (2021). Methionine restriction breaks obligatory coupling of cell proliferation and death by an oncogene Src in Drosophila. *Elife, 10*. doi:10.7554/eLife.59809

Okada, M., & Shi, Y. B. (2018). EVI and MDS/EVI are required for adult intestinal stem cell formation during postembryonic vertebrate development. *FASEB J, 32*(1), 431-439. doi:10.1096/fj.201700424R

Pietrocola, F., Galluzzi, L., Bravo-San Pedro, J. M., Madeo, F., & Kroemer, G. (2015). Acetyl coenzyme A: a central metabolite and second messenger. *Cell Metab, 21*(6), 805-821. doi:10.1016/j.cmet.2015.05.014

Prior, I. A., Lewis, P. D., & Mattos, C. (2012). A comprehensive survey of Ras mutations in cancer. *Cancer Res, 72*(10), 2457-2467. doi:10.1158/0008-5472.CAN-11-2612

Santabarbara-Ruiz, P., & Leopold, P. (2021). An Oatp transporter-mediated steroid sink promotes tumor-induced cachexia in Drosophila. *Dev Cell, 56*(19), 2741-2751 e2747. doi:10.1016/j.devcel.2021.09.009

Sasaki, A., Nishimura, T., Takano, T., Naito, S., & Yoo, S. K. (2021). white regulates proliferative homeostasis of intestinal stem cells during ageing in Drosophila. *Nat Metab, 3*(4), 546-557. doi:10.1038/s42255-021-00375-x

Serafini, T., Colamarino, S. A., Leonardo, E. D., Wang, H., Beddington, R., Skarnes, W. C., & Tessier-Lavigne, M. (1996). Netrin-1 is required for commissural axon guidance in the developing vertebrate nervous system. *Cell, 87*(6), 1001-1014. doi:10.1016/s0092-8674(00)81795-x

Silverio, R., Laviano, A., Rossi Fanelli, F., & Seelaender, M. (2011). l-carnitine and cancer cachexia: Clinical and experimental aspects. *J Cachexia Sarcopenia Muscle, 2*(1), 37-44. doi:10.1007/s13539-011-0017-7

Simon, M. A., Bowtell, D. D., Dodson, G. S., Laverty, T. R., & Rubin, G. M. (1991). Ras1 and a putative guanine nucleotide exchange factor perform crucial steps in signaling by the sevenless protein tyrosine kinase. *Cell, 67*(4), 701-716. doi:10.1016/0092-8674(91)90065-7

Song, W., Kir, S., Hong, S., Hu, Y., Wang, X., Binari, R., . . . Perrimon, N. (2019). Tumor-Derived Ligands Trigger Tumor Growth and Host Wasting via Differential MEK Activation. *Dev Cell, 48*(2), 277-286 e276. doi:10.1016/j.devcel.2018.12.003

Tang, A. H., Neufeld, T. P., Rubin, G. M., & Muller, H. A. (2001). Transcriptional regulation of cytoskeletal functions and segmentation by a novel maternal pair-rule gene, lilliputian. *Development, 128*(5), 801-813. doi:10.1242/dev.128.5.801

Tsuda-Sakurai, K., Kimura, M., & Miura, M. (2020). Diphthamide modification of eEF2 is required for gut tumor-like hyperplasia induced by oncogenic Ras. *Genes Cells, 25*(2), 76-85. doi:10.1111/gtc.12742

Villegas, S. N. (2019). One hundred years of Drosophila cancer research: no longer in solitude. *Dis Model Mech, 12*(4). doi:10.1242/dmm.039032

Wu, M., Pastor-Pareja, J. C., & Xu, T. (2010). Interaction between Ras(V12) and scribbled clones induces tumour growth and invasion. *Nature, 463*(7280), 545-548. doi:10.1038/nature08702

Yoo, S. K., Pascoe, H. G., Pereira, T., Kondo, S., Jacinto, A., Zhang, X., & Hariharan, I. K. (2016). Plexins function in epithelial repair in both Drosophila and zebrafish. *Nat Commun, 7*, 12282. doi:10.1038/ncomms12282

Fig 1

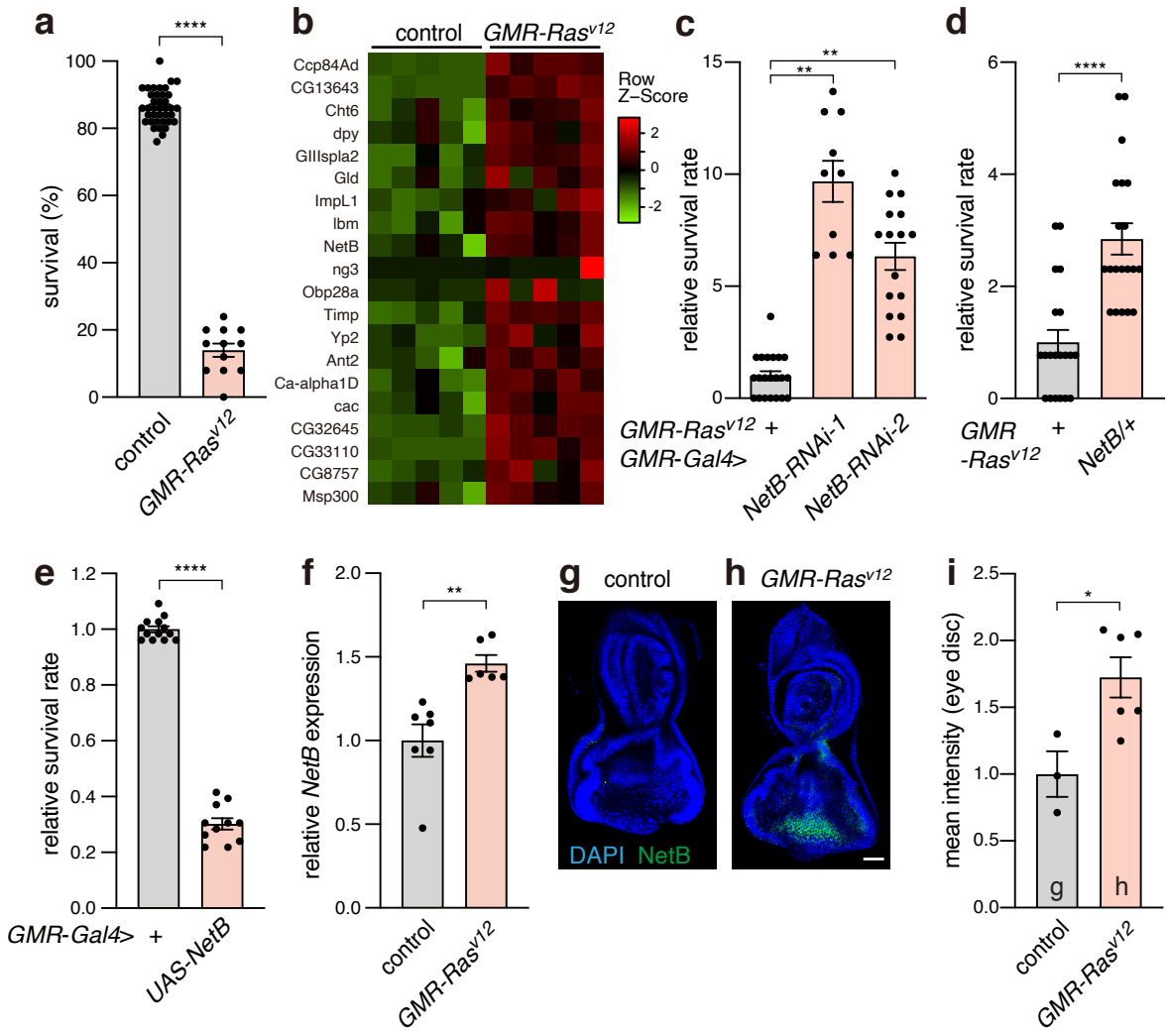
a
survival (%)
control
GMR-Ras^v12
b
control
GMR-Ras^v12
Row Z-Score
Ccp84Ad
CG13643
Cht6
dpy
GIIIspla2
Gld
ImpL1
lbm
NetB
ng3
Obp28a
Timp
Yp2
Ant2
Ca-alpha1D
cac
CG32645
CG33110
CG8757
Msp300
c
relative survival rate
GMR-Ras^v12 +
GMR-Gal4>
NetB-RNAi-1
NetB-RNAi-2
d
relative survival rate
GMR -Ras^v12 +
NetB/+
e
relative survival rate
GMR-Gal4> +
UAS-NetB
f
relative NetB expression
control
GMR-Ras^v12
g control
h GMR-Ras^v12
DAPI NetB
i
mean intensity (eye disc)
g
h
control
GMR-Ras^v12

Fig 2

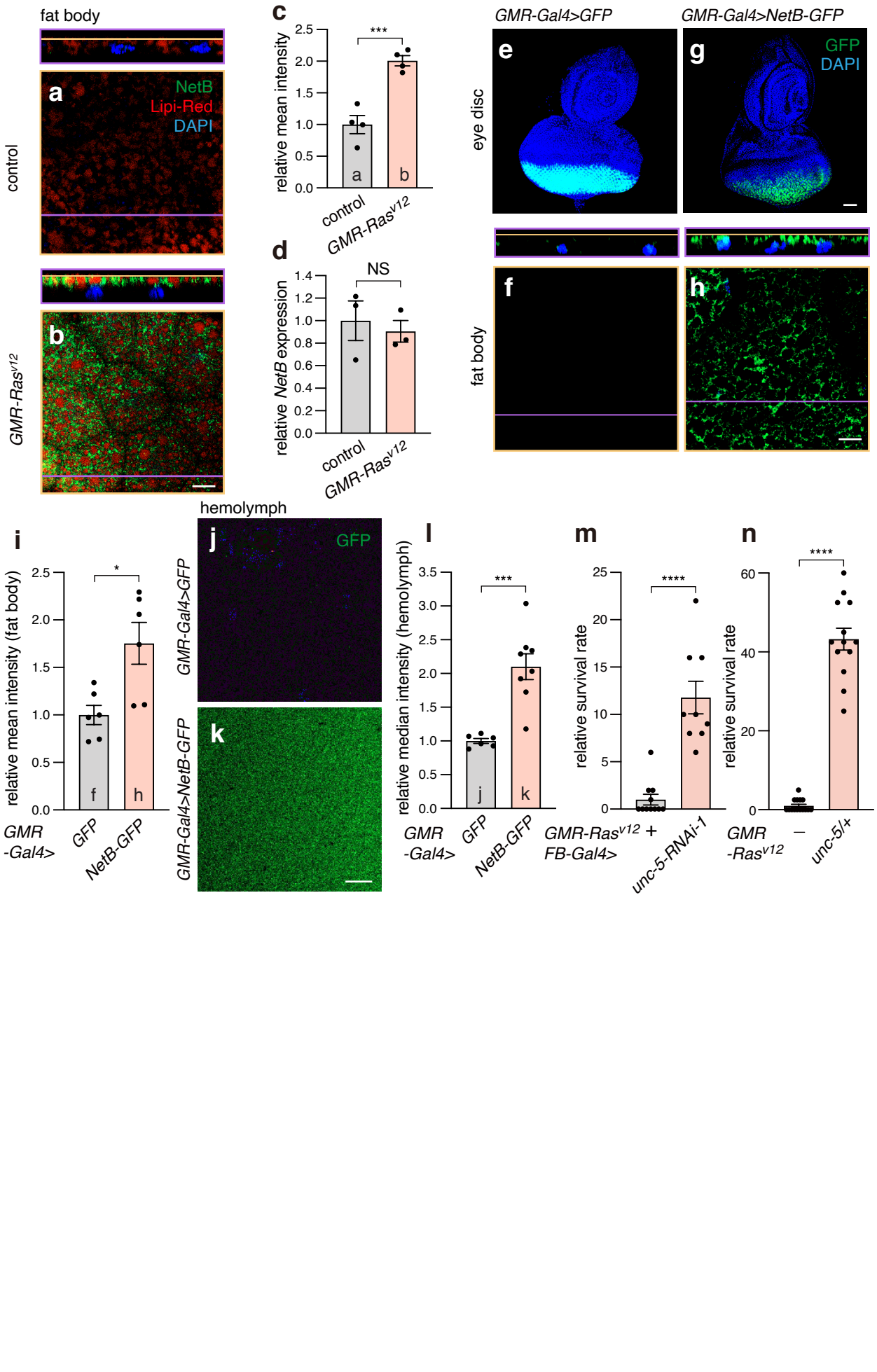
fat body
control
GMR-Ras^v12
a
b
NetB
Lipi-Red
DAPI
c
relative mean intensity
***
control
GMR-Ras^v12
d
relative NetB expression
NS
GMR-Gal4>GFP
GMR-Gal4>NetB-GFP
e
g
GFP
DAPI
eye disc
f
h
fat body
hemolymph
i
relative mean intensity (fat body)
*
GMR -Gal4>
GFP
NetB-GFP
j
k
GFP
GMR-Gal4>GFP
GMR-Gal4>NetB-GFP
l
relative median intensity (hemolymph)
***
m
relative survival rate
****
GMR-Ras^v12 + FB-Gal4>
unc-5-RNAi-1
n
relative survival rate
****
GMR -Ras^v12
unc-5/+

Fig 3

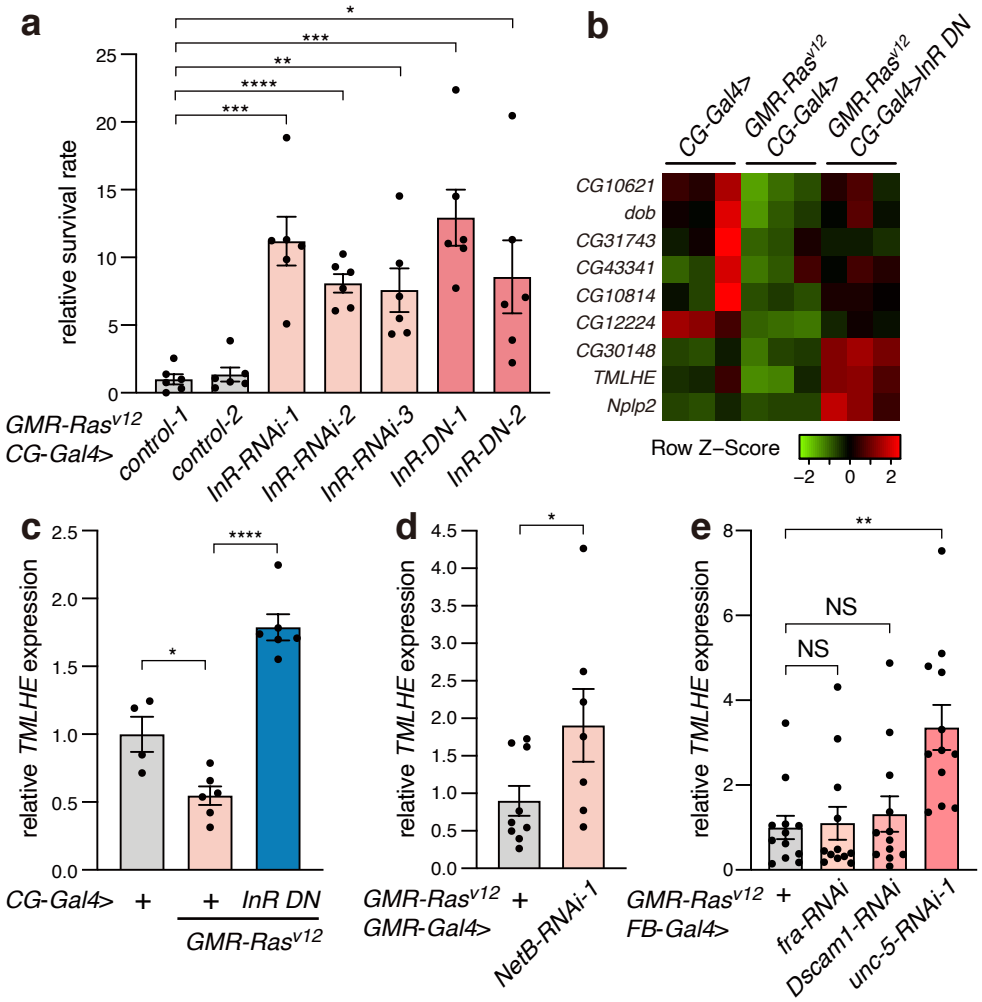
a
relative survival rate
GMR-Ras^v12
CG-Gal4>
control-1
control-2
InR-RNAi-1
InR-RNAi-2
InR-RNAi-3
InR-DN-1
InR-DN-2
b
CG-Gal4>
GMR-Ras^v12 CG-Gal4>
GMR-Ras^v12 CG-Gal4>InR DN
CG10621
dob
CG31743
CG43341
CG10814
CG12224
CG30148
TMLHE
Nplp2
Row Z−Score
c
relative TMLHE expression
CG-Gal4> + + InR DN
GMR-Ras^v12
d
relative TMLHE expression
GMR-Ras^v12 + NetB-RNAi-1
GMR-Gal4>
e
relative TMLHE expression
NS
NS
GMR-Ras^v12 +
FB-Gal4>
fra-RNAi
Dscam1-RNAi
unc-5-RNAi-1

Fig 4

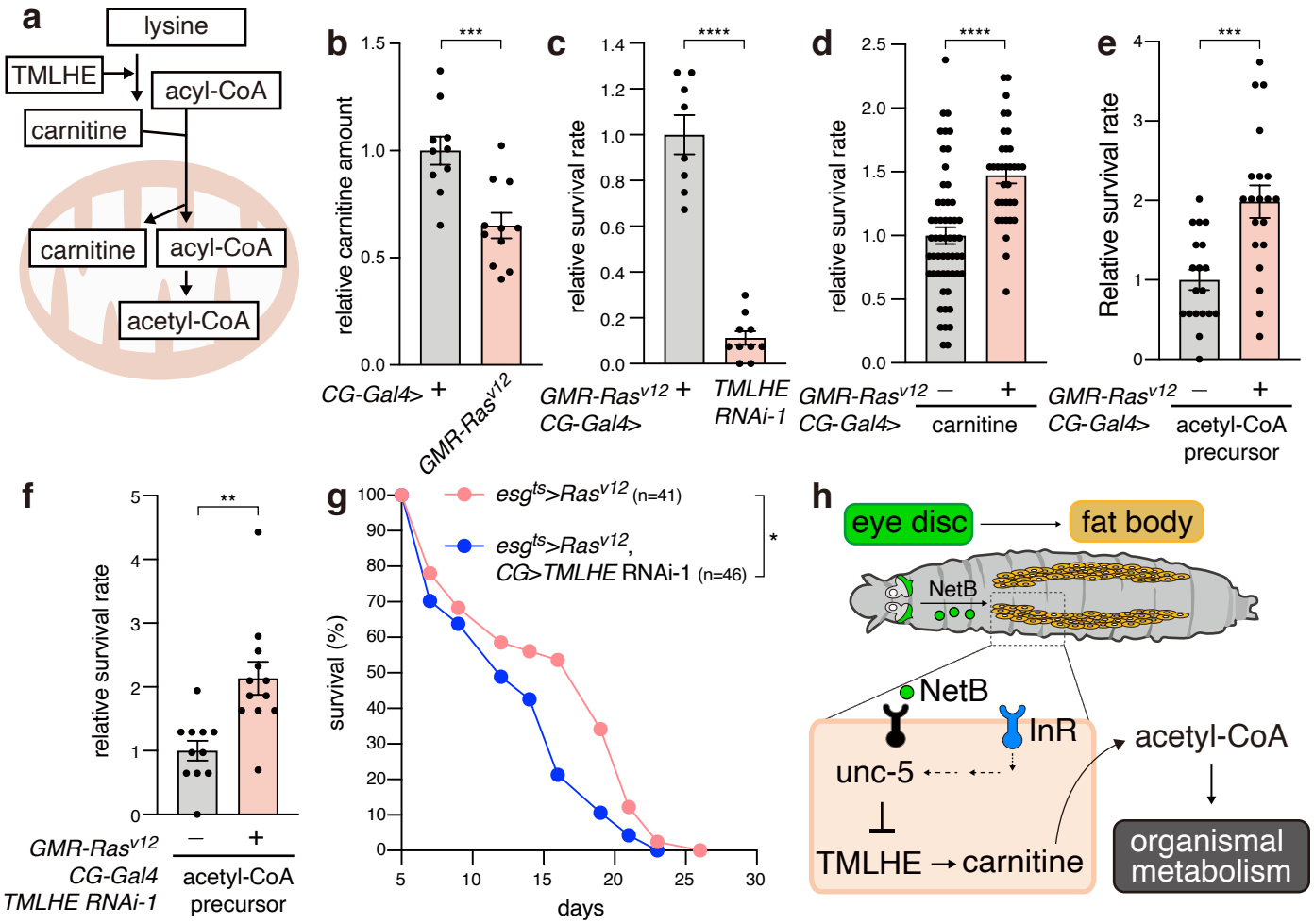
a
lysine
TMLHE
acyl-CoA
carnitine
carnitine
acyl-CoA
acetyl-CoA
b
relative carnitine amount
***
CG-Gal4> +
GMR-Ras^v12
c
relative survival rate
****
GMR-Ras^v12 +
CG-Gal4>
TMLHE
RNAi-1
d
relative survival rate
****
GMR-Ras^v12 CG-Gal4>
– carnitine +
e
Relative survival rate
***
GMR-Ras^v12 CG-Gal4>
– acetyl-CoA precursor +
f
relative survival rate
**
GMR-Ras^v12
CG-Gal4
TMLHE RNAi-1
– acetyl-CoA precursor +
g
esg^ts>Ras^v12 (n=41)
esg^ts>Ras^v12, CG>TMLHE RNAi-1 (n=46)
*
survival (%)
days
h
eye disc
fat body
NetB
NetB
InR
unc-5
TMLHE → carnitine
acetyl-CoA
organismal metabolism

Fig S1

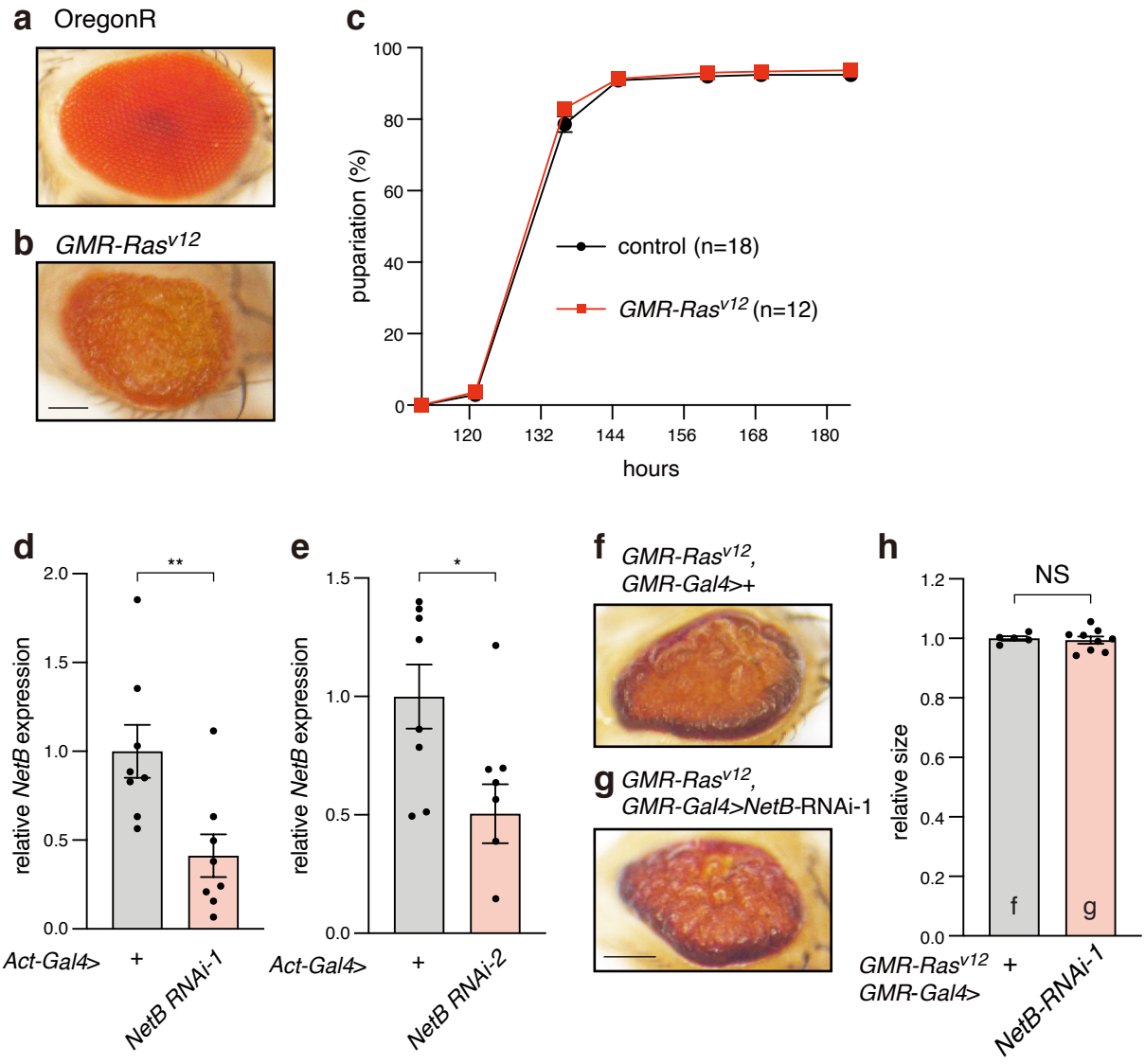
a OregonR
b GMR-Ras^{v12}
c
pupariation (%)
hours
control (n=18)
GMR-Ras^{v12} (n=12)
d
relative NetB expression
Act-Gal4>
+
NetB RNAi-1
e
relative NetB expression
Act-Gal4>
+
NetB RNAi-2
f GMR-Ras^{v12}, GMR-Gal4>+
g GMR-Ras^{v12}, GMR-Gal4>NetB-RNAi-1
h
NS
relative size
f
g
GMR-Ras^{v12} GMR-Gal4>
+
NetB-RNAi-1

Fig S2

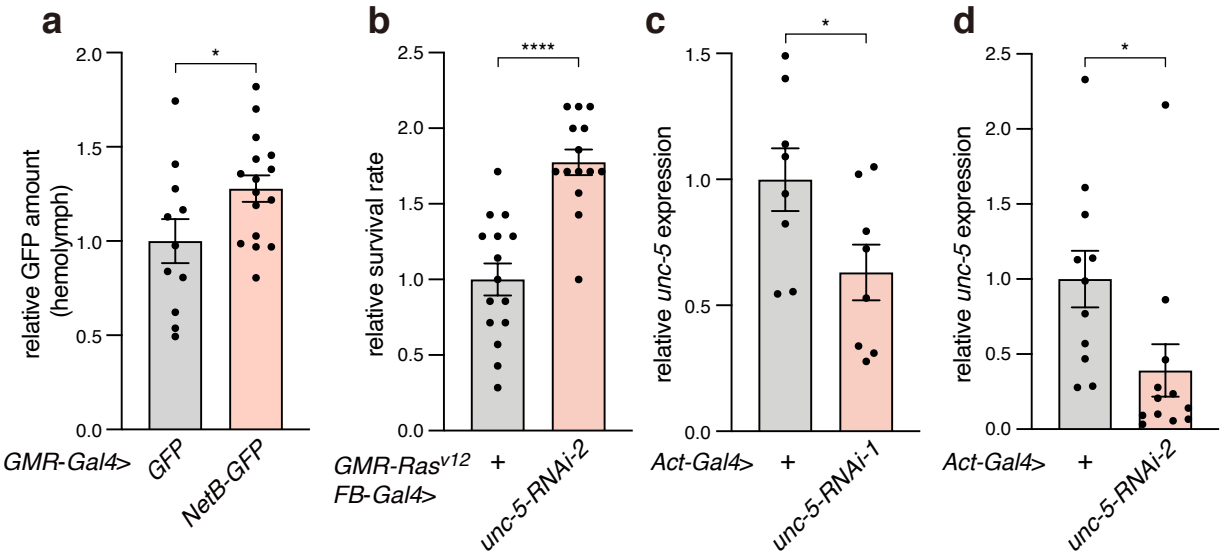
a
b
c
d
relative GFP amount (hemolymph)
relative survival rate
relative unc-5 expression
relative unc-5 expression
*
****
*
*
GMR-Gal4>
GFP
NetB-GFP
GMR-Ras^v12 FB-Gal4>
+
unc-5-RNAi-2
Act-Gal4>
+
unc-5-RNAi-1
Act-Gal4>
+
unc-5-RNAi-2

Fig S3

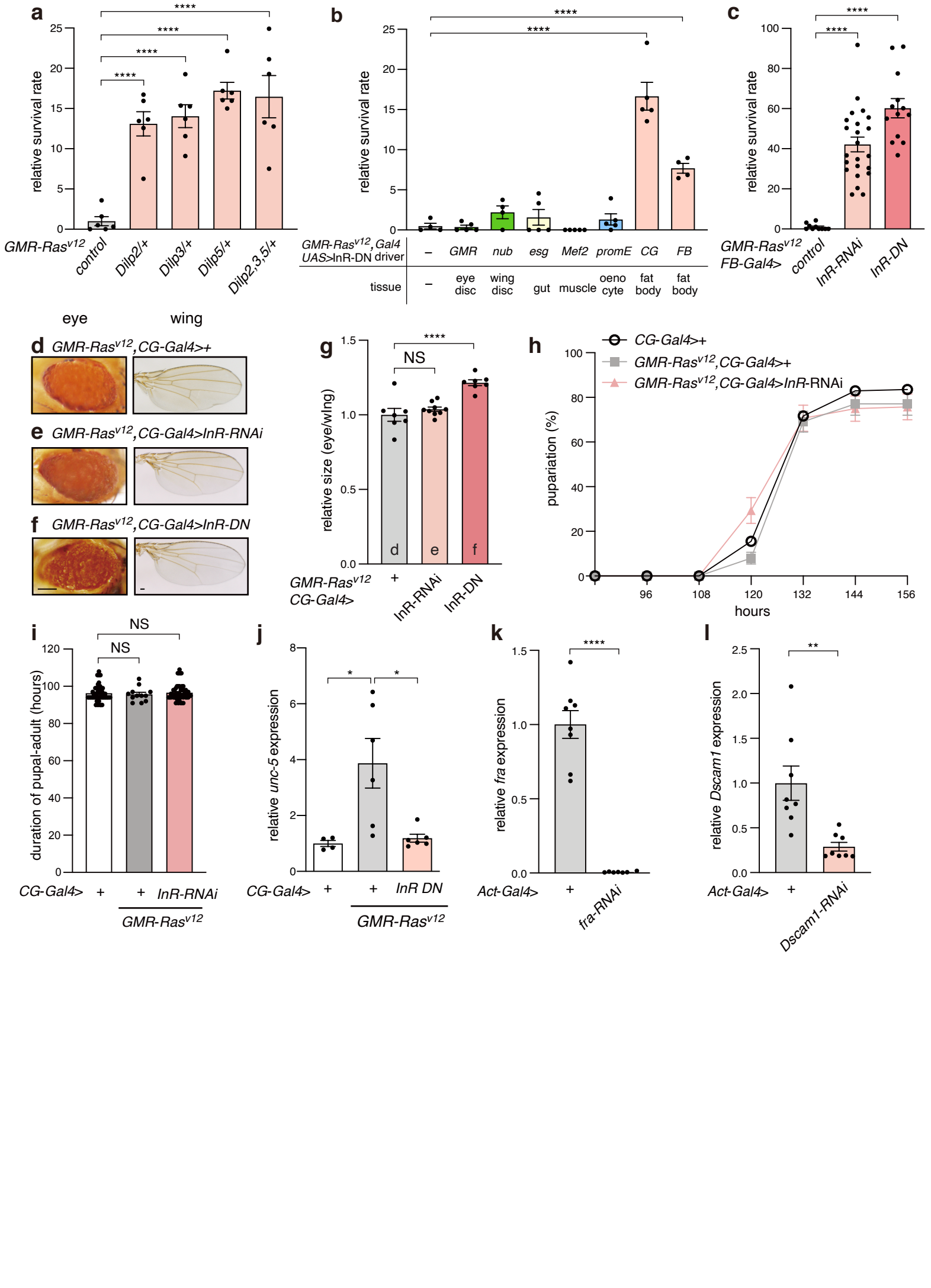
a
relative survival rate
GMR-Ras^{v12}
control
Dilp2/+
Dilp3/+
Dilp5/+
Dilp2,3,5/+
b
relative survival rate
GMR-Ras^{v12},Gal4
UAS>InR-DN driver
–
GMR
nub
esg
Mef2
promE
CG
FB
tissue
–
eye disc
wing disc
gut
muscle
oeno cyte
fat body
fat body
c
relative survival rate
GMR-Ras^{v12}
FB-Gal4>
control
InR-RNAi
InR-DN
eye
wing
d GMR-Ras^{v12},CG-Gal4>+
e GMR-Ras^{v12},CG-Gal4>InR-RNAi
f GMR-Ras^{v12},CG-Gal4>InR-DN
g
relative size (eye/wing)
NS
d
e
f
GMR-Ras^{v12}
CG-Gal4>
+
InR-RNAi
InR-DN
h
CG-Gal4>+
GMR-Ras^{v12},CG-Gal4>+
GMR-Ras^{v12},CG-Gal4>InR-RNAi
pupariation (%)
hours
i
duration of pupal-adult (hours)
NS
NS
CG-Gal4>
+
+
InR-RNAi
GMR-Ras^{v12}
j
relative unc-5 expression
CG-Gal4>
+
+
InR DN
GMR-Ras^{v12}
k
relative fra expression
Act-Gal4>
+
fra-RNAi
l
relative Dscam1 expression
Act-Gal4>
+
Dscam1-RNAi

Fig S4

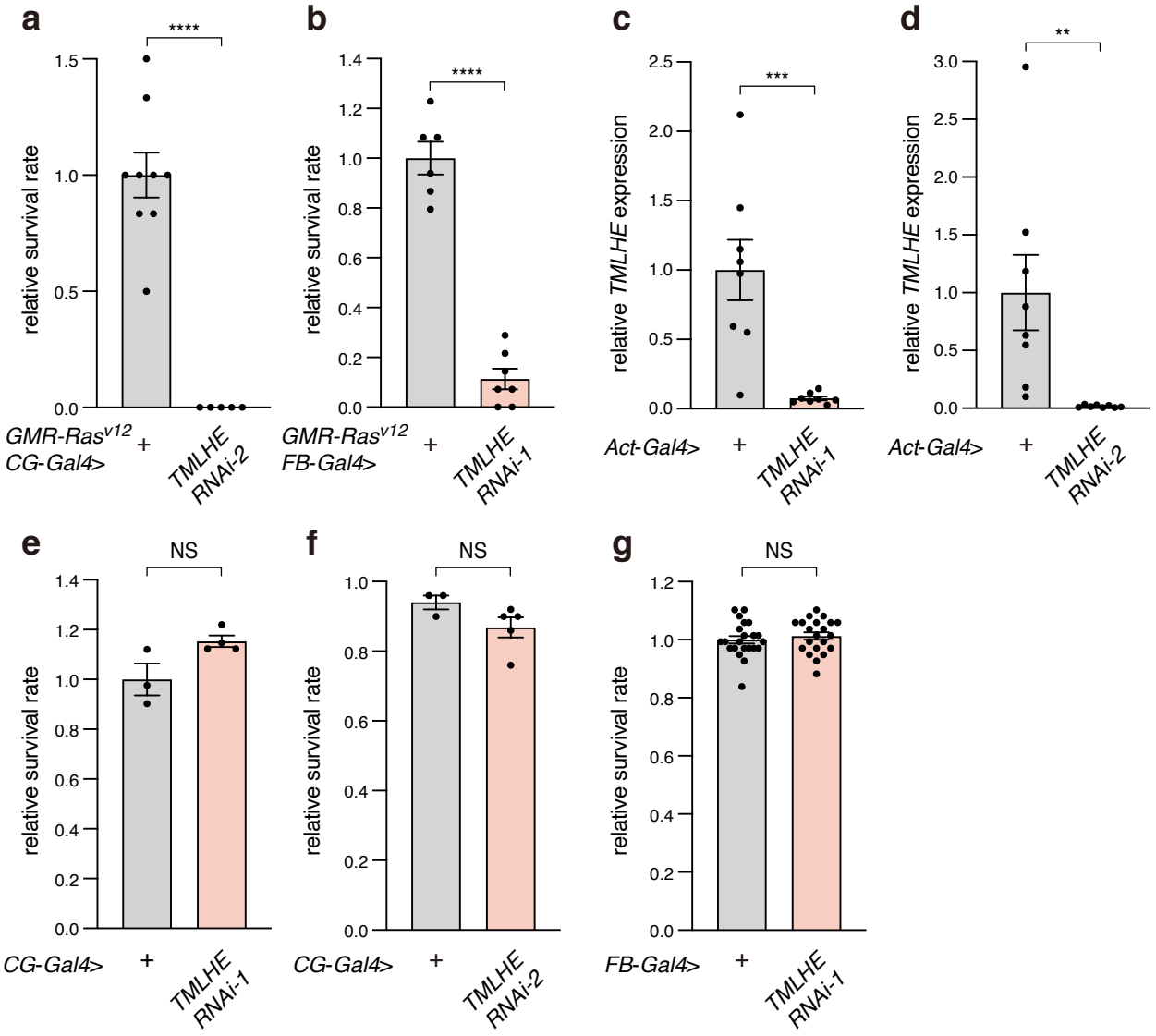
a
****
relative survival rate
1.5
1.0
0.5
0.0
GMR-Ras^v12
CG-Gal4>
+
TMLHE
RNAi-2
b
****
relative survival rate
1.4
1.2
1.0
0.8
0.6
0.4
0.2
0.0
GMR-Ras^v12
FB-Gal4>
+
TMLHE
RNAi-1
c
***
relative TMLHE expression
2.5
2.0
1.5
1.0
0.5
0.0
Act-Gal4>
+
TMLHE
RNAi-1
d
**
relative TMLHE expression
3.0
2.5
2.0
1.5
1.0
0.5
0.0
Act-Gal4>
+
TMLHE
RNAi-2
e
NS
relative survival rate
1.4
1.2
1.0
0.8
0.6
0.4
0.2
0.0
CG-Gal4>
+
TMLHE
RNAi-1
f
NS
relative survival rate
1.0
0.8
0.6
0.4
0.2
0.0
CG-Gal4>
+
TMLHE
RNAi-2
g
NS
relative survival rate
1.2
1.0
0.8
0.6
0.4
0.2
0.0
FB-Gal4>
+
TMLHE
RNAi-1

Fig S5

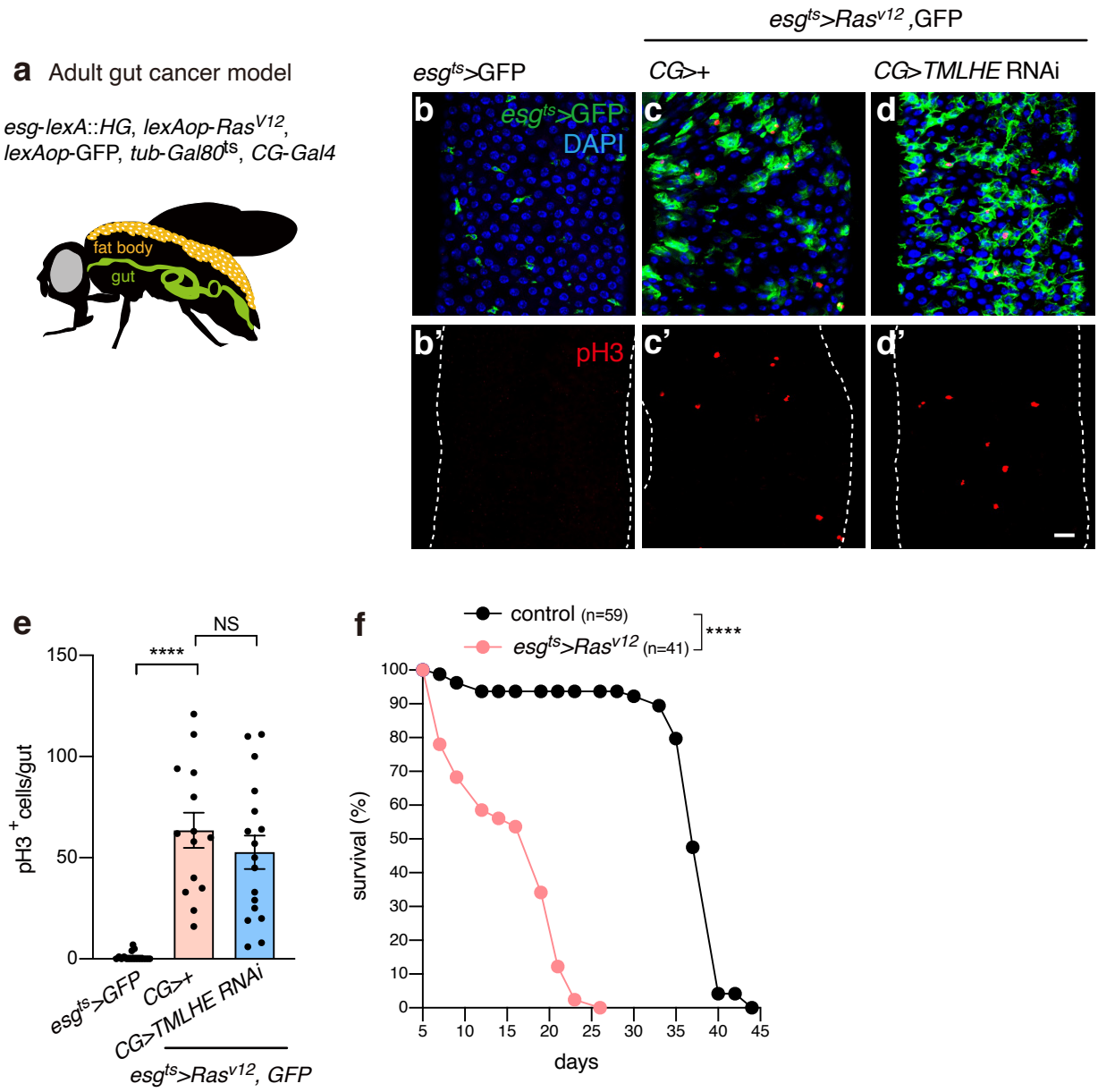
a Adult gut cancer model
esg-lexA::HG, lexAop-Ras^V12, lexAop-GFP, tub-Gal80^ts, CG-Gal4
fat body
gut
esg^ts>Ras^v12 ,GFP
esg^ts>GFP
CG>+
CG>TMLHE RNAi
b esg^ts>GFP DAPI
c
d
b' pH3
c'
d'
e
NS
****
150
100
50
0
pH3 + cells/gut
esg^ts>GFP
CG>+
CG>TMLHE RNAi
esg^ts>Ras^v12, GFP
f
control (n=59)
esg^ts>Ras^v12 (n=41)
****
survival (%)
days